J Radioanal Nucl Chem (2017) 312:187–198
DOI 10.1007/s10967-017-5209-y

Adsorptive removal of uranyl ions in aqueous solution using hydrothermal carbon spheres functionalized with 4-aminoacetophenone oxime group

Zhiyang Zheng[1,3] · Youqun Wang[1] · Wuwei Zhao[1,3] · Guoxuan Xiong[1,3] · Xiaohong Cao[1,3] · Ying Dai[1,3] · Zhanggao Le[1,3] · Shenglong Yu[1,3] · Zhibin Zhang[1,2,3] · Yunhai Liu[1,3]

Received: 28 September 2016 / Published online: 18 March 2017

Abstract Hydrothermal carbon spheres (HCSs) functionalized with 4-aminoacetophenone oxime group (HCSs-oxime) were prepared by a grafting method and explored to adsorption of uranyl ions from aqueous solution. The results of FT-IR, elemental analysis and zeta potential indicate a successfully modification with oxime group. The adsorbent shows an excellent adsorption capacity (Langmuir, $q_m = 588.2$ mg g^{-1}) and quick adsorption kinetic (equilibrium time of approximately 60 min) at optimal pH of 6.0. The adsorptive selectivity for uranyl ions has been also great improved in present with various co-existing ions. Overall, HCSs-oxime is a potentially promising material for selective removal of uranium in the contaminated solution.

Keywords Functionalization · Hydrothermal carbon spheres · Uranyl ions · Adsorption

✉ Zhibin Zhang
zhang_ecut@hotmail.com

✉ Yunhai Liu
Walton_liu@163.com

[1] Fundamental Science on Radioactive Geology and Exploration Technology Laboratory, East China University of Technology, Nanchang 330013, Jiangxi, China

[2] Engineering Research Center of Nuclear Technology Application (East China University of Technology), Ministry of Education, Nanchang 330013, Jiangxi, China

[3] State Key Laboratory Breeding Base of Nuclear Resources and Environment, East China University of Technology, Nanchang 330013, Jiangxi, China

Introduction

Uranium is a significant radioactive nuclide which is widely utilized in nuclear industry [1]. Meanwhile, uranium has a great harmful influence on the eco-system and human beings when it releases into the aqueous solution for its radioactivity and heavy metallic toxicity. In the aquatic environment, uranium is always in the form of uranyl ion (UO_2^{2+}) which is water-soluble and easily mobile. Therefore, removal and recovery of uranyl ion from aqueous solution is of great importance for not only sustainable development of nuclear energy but also environment protection.

Hitherto, numerous techniques have been developed for recycling of uranyl ions from water solution, such as ion exchange [2], solvent extraction [3], chemical precipitation [4], membrane processes [5] and adsorption [6], etc. Among all of these means mentioned above, adsorption has been supposed as one of most effective and promising ways. For the radioactive contamination with low concentration uranium, adsorption shows its superiority of fast removal rate, easy operation, and low cost, etc. [7, 8].

In the past few decades, large series of adsorbents have been prepared and utilized for getting rid of uranium in the aqueous solution, including carbonaceous material [9, 10], polymer [11, 12] and clay minerals [13, 14]. Of these adsorbents, carbonaceous adsorbents have drawn increasing attention for their irradiation and chemical stability. Hydrothermal carbon spheres (HCSs), an emerging style of carbonaceous adsorbent [15], is prepared through various types of carbohydrates [16, 17]. HCSs with well-behaved features of rule structure has synthesized without calcination at high temperature comparing with traditional activated carbon. However, fewer specific functional groups on

the surface have restrained the application of HCSs in adsorption of uranyl ions from the aqueous solution. The capacity and selectivity of the HCSs has been significantly increased once grafting of purposeful group involving of carboxyl [18] and phosphate [19] and oxime [20]. For those functional group, oxime is an exceptional chelating group showing substantial affinity toward uranyl ions [21]. Though the amido-oxime group has been extensively employed to modify of hydrothermal carbon materials for removal of uranyl ions [22], 4-aminoacetophenone oxime, with similar structure to the amido-oxime, has not been applied to anchor on the surface of HCSs. In light of these motivations, it would be an effective adsorbents of HCSs functionalized with 4-aminoacetophenone oxime for selective preconcentration of uranyl ions from the aqueous solution.

Therefore, in this study, 4-aminoacetophenone oxime group has been introduced onto HCSs by a grafting method to enhance the adsorption ability for uranyl ion. The functional groups and micro morphology as well as composition of the adsorbents of HCSs and HCSs-oxime has been characterized by FT-IR, SEM and elemental analyzer, respectively. Adsorption of UO_2^{2+} in aqueous solution by pristine and decorated HCSs also has been comprehensively investigated to optimize the influence of various factors including of solution pH, contact time and initial concentration of uranium as well as temperature. Moreover, the thermodynamics, kinetics along with isothermals of adsorption processes were systematically explored. Finally, the adsorptive selectivity of HCSs and HCSs-oxime for uranyl ions has been experimented in the solution with several co-existing ions of Mg^{2+}, Na^{+}, Zn^{2+}, Mn^{2+}, Co^{2+}, Ni^{2+}, Sr^{2+}, Cs^{+}, and Hg^{2+}.

Experimental

Materials

4-Aminoacetophenone and *N*, *N*′-dicyclohexylcarbodiimide (DCC) were purchased from Aladdin Chemistry Co., Ltd. All the chemical reagents were of analytical grade without further purification.

A stock UO_2^{2+} solution was prepared according to the [23]: 20 mL hydrochloric acid ($\rho = 1.18$ g mL^{-1}), 2 mL 30% hydrogen peroxide were added into a 100 mL beaker containing of 1.1792 g U_3O_8 successively. The mixture was heated up to nearly waterless and then 10 mL nitric acid ($\rho = 1.42$ g mL^{-1}) was put into the beaker. The solution transferred to a 1000 mL volumetric flask was diluted to the mark line with distilled water to gain a UO_2^{2+} stock solution (1.0 mg mL^{-1}).

Preparation of carboxylated hydrothermal carbon spheres (HCSs-COOH)

Typically, the glucose solution (80 mL, 20 wt%) was transferred into a 100 mL Teflon-lined stainless steel autoclave, and heated at 453 K with a rate of 2.5 °C min^{-1} and maintained for 24 h. Then obtained hydrothermal carbon were washed with deionized water, ethanol and acetone and dried at 323 K in vacuum. Afterward, the HCSs were calcined at 573 K in a muffle furnace for 3 h to obtain carboxylated HCSs (HCSs-COOH) [24].

Synthesis of 4-aminoacetophenone oxime

The solution containing of 2.00 g 4-aminoacetophenone dissolved in 55 mL ethanol and 1.03 g $NH_2OH{\cdot}HCl$ and 0.78 g Na_2CO_3 dissolved in 20 mL deionized water were refluxed for 3 h. The yellow crystal of 4-aminoacetophenone oxime is obtained after removing of solvent by rotary evaporation [25].

Preparation of 4-aminoacetophenone oxime hydrothermal carbon spheres

1.0 g HCSs-COOH was added into a 250 mL flask with 40.0 mL ethyl acetate under stirring in ice bath until the powder homogenization. Afterward, 1.0 g DCC and 0.6 g 4-aminoacetophenone oxime was added sequently under continue stirring for 30 min. Subsequently, the solution was stirred continuously for 24 h in room temperature, and the product was filtrated and washed with deionized water and ethanol and then dried at 323 K in a vacuum for 8 h to get HCSs-oxime (Scheme 1).

Adsorption experiments

The adsorption studies of uranyl ion in the aqueous solution on HCSs and HCSs-oxime were carried out as follows. Typically, 0.01 g of sorbents was added into a 100 mL solution containing uranyl ions with different initial concentration and pH (adjusted with 0.1 mol L^{-1} HCl and 0.1 mol L^{-1} NaOH). The concentration of UO_2^{2+} in the solution was determined by the arsenazo-III method with a 721 type spectrophotometer at 650 nm [26]. And the concentrations of co-existing ions Mg^{2+}, Na^{+}, Zn^{2+}, Mn^{2+}, Co^{2+}, Ni^{2+}, Sr^{2+}, Cs^{+}, and Hg^{2+} were analyzed by inductively coupled plasma optical emission spectrometer. Sorption amount q_e (mg g^{-1}) and distribution coefficient K_d can be calculated by the following equations [27]:

$$q_e = \frac{(C_0 - C_e)V}{m}, \quad (1)$$

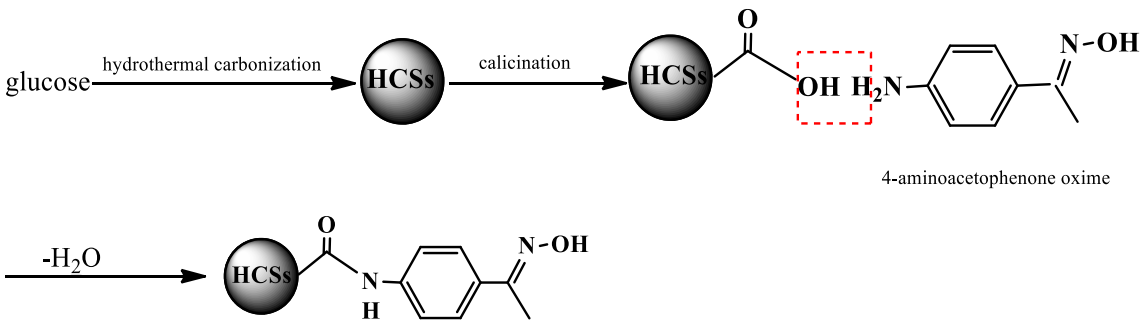

Scheme 1 Graphical synthetic routes of HCSs-oxime [24]

$$K_d = \frac{(C_0 - C_e)}{C_e} \times \frac{V}{m}, \quad (2)$$

where C_0 and C_e are the initial and equilibrium concentration of uranium (mg L^{-1}), respectively, V is the volume of test solution (L), m is the mass of sorbent (g). All of the batch adsorption experiments were conducted three times, and the average values were chosen.

Determining of uranyl ion by arsenazo-III spectrophotometry

The UV–vis spectra of arsenazo-III and the complexes of arsenazo-III–U in the wavelength range from 400 to 900 nm are presented in Fig. 1. It is easily seen that, there is a new peak appeared at 650 nm aparting from 520 nm, which is the characteristic peak of arsenazo-III–U, thus 650 nm is been identified as maximum absorption wavelength for analyze of uranium in the aqueous solution.

The arsenazo-III method in analyzing uranium is briefly described as follow: 5 mL solution after adsorption was taken off and separate from solid by centrifugation. Then 1 mL suspension was added to 25 mL volumetric flask.

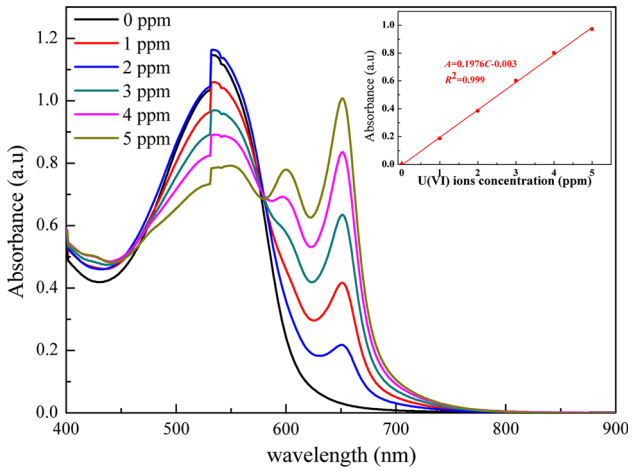

Fig. 1 The UV–vis spectra of uranyl ions with arsenazo-III [*inset* calibration plot of the arsenazo III–uranium complex vs. the concentrations of the U(VI)]

Afterwards, three drops of 3 mol L^{-1} HNO_3 was added to the solution. Then 2 mL buffer solution (chloroacetic acid–sodium acetate, pH 2.5) and 2 mL arsenazo-III solution was placed into the mixture sequentially. Finally, the absorbance of the solutions has been measured at the maximum wavelength of 650 nm by a 721 type spectrophotometer. The adsorbances at the 650 nm in the uranium concentration range of 0–5 ppm increase gradually from 0.031 to 1.033. The linear correlation coefficient of calibration curve shown in Fig. 1 (inset) is over 0.999 indicating that the absorbance at 650 nm are proportional to the concentration. Accordingly, the arsenazo-III method can be used in analyzing uranium.

Characterization

Surface morphology was characterized by scanning electron microscopy (SEM, FEI Company, Oregon, USA). The FT-IR spectrum was recorded with a Nicolet i380 spectator in the wavenumber range of 550–3600 cm^{-1}. The contents of carbon, hydrogen, oxygen, and nitrogen in the samples were determined by an elemental analyzer (Carlo-Erba 1106, Italy). The zeta potential was measured using a Particle Metrix flowing current potential analyzer (Stabino, German).

Results and discussion

SEM

The SEM images of pristine–HCSs and HCSs-oxime in the Fig. 2 displayed that the spheres structure still maintained after 4-aminoacetophenone oxime grafting. Furthermore, the particle size and their distribution of HCSs and HCSs-oxime shown in the Fig. 2 (inset) were analyzed by the software of Nano Measure 1.2. It can be seen, the dimension of HCSs and HCSs-oxime is in the range of 0.3–0.8 μm, and the average diameter of HCSs and HCSs-oxime is 0.52 and 0.58 μm, respectively. The results above indicate

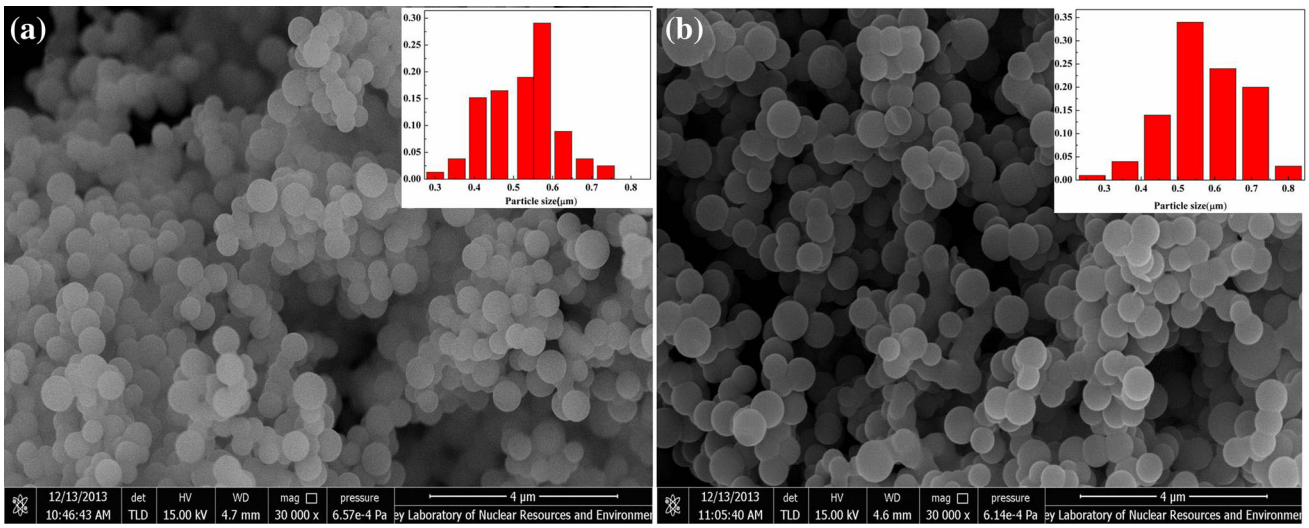

Fig. 2 SEM images of HCSs (**a**) and HCSs-oxime (**b**) (*inset* shows the particle size distribution)

that the sphere structure has not changed after modification of 4-aminoacetophenone oxime group.

FT-IR

The FT-IR spectra of the pristine–HCSs, HCSs-COOH and HCSs-oxime are presented in Fig. 3. The peaks at 3400 cm^{-1} are assigned to the stretching vibrations of O–H or N–H groups [28]. Peaks emerged at 1710 and 1619 cm^{-1} is corresponding to C=O and C=C stretching vibrations [29], respectively. A new peak appeared at 1257 cm^{-1} in the Fig. 3b can be associated with C–O vibration of carboxylic acid anhydride, which suggested that carboxyl were introduced in HCSs (Fig. 3b). New bands of C=N, N–H and N–O can be observed at 1623, 1575 and 932 cm^{-1} in the Fig. 3c [30]. The results imply that oxime group was successfully grafting on the surface of HCSs.

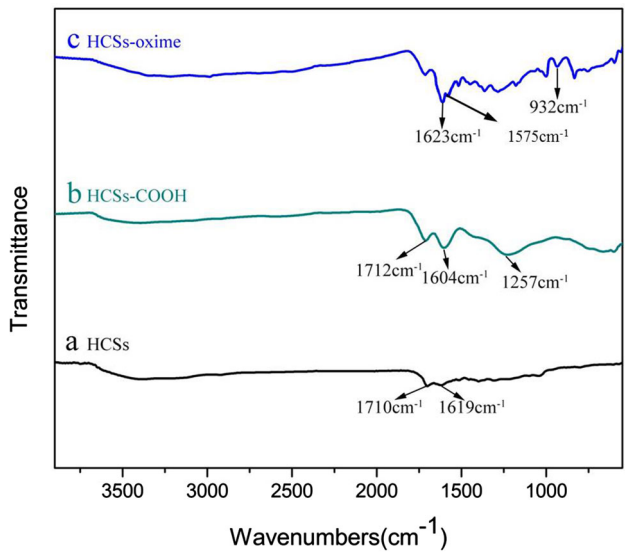

Fig. 3 FT-IR spectra for HCSs after graftation of COOH and oxime groups

Elemental analysis

The contents of C, H, O, and N in the unmodified and modified HCSs have been determined by element analysis. As shown in Table 1, the mass percent of nitrogen increases from 0.28% (pristine–HCSs) to 7.46% after functionalization, indicating that the oxime groups were grafted onto the surface of HCSs. The amount of oxime groups was calculated based on the increment of the content of nitrogen to be approximately 2.56 mmol g^{-1}.

Zeta potential

As shown in Fig. 4, the zeta potential of HCSs and HCSs-oxime decreased with the increasing of solution pH. At lower pH, the zeta potential of HCSs-oxime is more positive than HCSs due to the protonation degree of N in the oxime groups. While, the zeta potential of HCSs-oxime is more negative than HCSs at higher pH, it is attributed to the ionization of N [31]. Furthermore, the point of zero change of HCSs-oxime ($pH_{PZC} = 3.60$) was lower than HCSs ($pH_{PZC} = 3.28$), which was due to the 4-aminoacetophenone oxime group introduction on the surface of HCSs-oxime.

Table 1 Element analysis of HCSs and HCSs-oxime

Adsorbents	C (%)	N (%)	H (%)	O (%)
HCSs	73.45	0.28	4.71	21.56
HCSs-oxime	64.12	7.46	5.14	23.28

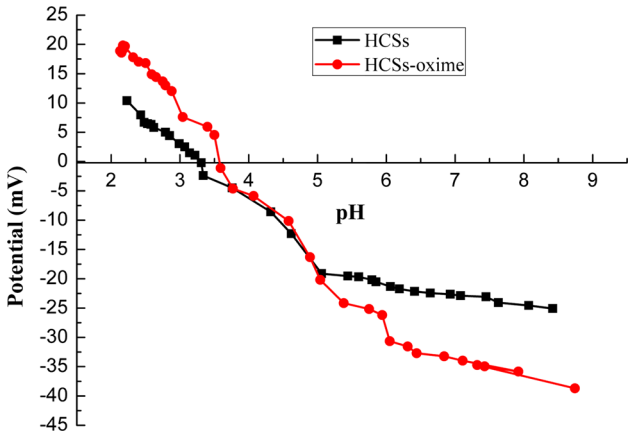

Fig. 4 Zeta potential of HCSs and HCSs-oxime as a function of pH

Effect of pH

The pH values of solution have a great effect on the uranium species distribution and the surface charge of adsorbents [32]. Consequently, the solution pH values are extremely crucial parameters for adsorption of uranyl ions by HCSs and HCSs-oxime. The effects of pH on UO_2^{2+} adsorption onto HCSs and HCSs-oxime were carried out over the pH range 3.0–8.0 using 50 mg L^{-1} initial uranium concentration at 298 K. The results displayed in Fig. 5, the uranium amounts adsorbed on HCSs and HCSs-oxime increase with the increasing initial solution pH from 3.0 to 6.0, and reach the maximum at pH of 6.0 then start to decrease. The smaller adsorption capacity at lower pH value could be attributed to the hydroxyl groups of 4-aminoacetophenone oxime on the adsorbents will be highly protonized, resulting in decreasing the oxime's nucleophilicity towards U(VI) and limiting the U(VI) sorption onto the sorbents [33]. With the increasing solution pH, the protonation degree of the 4-aminoacetophenone oxime group will be decreased, and the surface charge could become negative, thus promote the adsorption. As the pH of solution increased over 6.0, the hydroxide products of UO_2^{2+} such as $UO_2(OH)_3^-$ and $(UO_2)_3(OH)_7^-$ appeared [34], lead to generated electrostatic repulsion between these anions with the adsorbents. Thus, inhibited the adsorption of UO_2^{2+} by sorbents and caused the adsorption capacity decreased gradually. Therefore, the solution pH value of 6 was elected as the optimal pH for the sorption of UO_2^{2+} onto HCSs and HCSs-oxime, and used for the subsequent experiments. In addition, uranium adsorbed amount is significantly improved from 55.7±1.5 to 366.8±16.0 mg g^{-1} at optimal pH after functionalization with 4-aminoacetophenone oxime group on the surface of HCSs.

Effect of sorbent dosage

As shown in Fig. 6, the amount of U(VI) sorbed on HCSs-oxime declined from 360.7 ± 10.9 to 96.2 ± 3.3 mg g^{-1} with the increasing of dosage from 0.1 to 0.5 g L^{-1}. Hence, in this study, the dosage of the adsorbent is determined to be 0.1 g L^{-1}.

Sorption kinetics

The UO_2^{2+} uptake on HCSs and HCSs-oxime are shown in Fig. 7 as the function of contact time varying from 0 to 180 min at the initial uranium concentration of 50 mg L^{-1} and the sorbents dosage of 10 mg. It can be seen that the process of adsorption reached equilibrium only in 60 min. The fast adsorption rate at the beginning of the process may

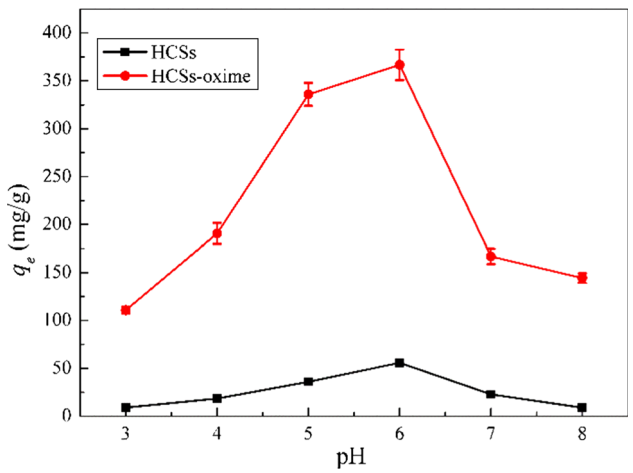

Fig. 5 The effect of pH on the UO_2^{2+} sorption by HCSs and HCSs-oxime (C_0 = 50 mg L^{-1}, t = 60 min, V = 100 mL, T = 298.15 K, and m = 10 mg)

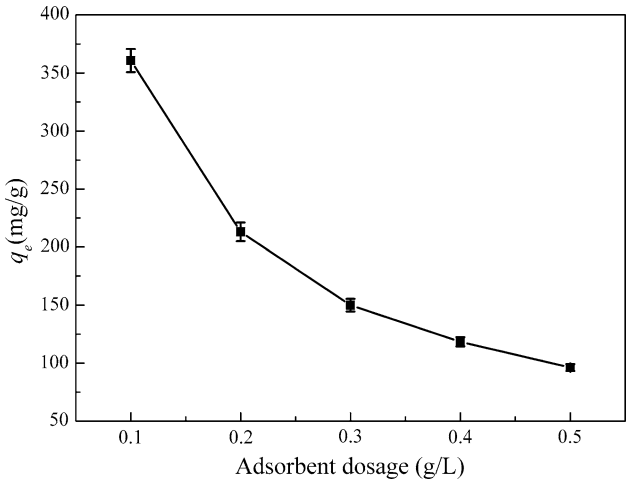

Fig. 6 Effect of sorbent dosage on the UO_2^{2+} sorption by HCSs-oxime (C_0 = 50 mg L^{-1}, pH 6.0, t = 60 min, V = 100 mL, T = 298.15 K)

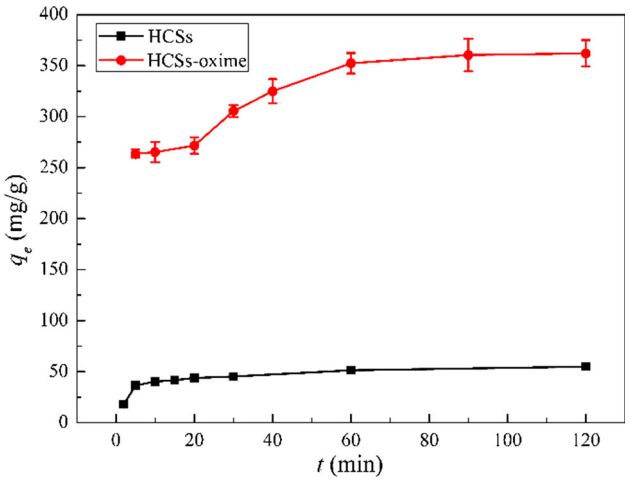

Fig. 7 Effects of contact time on UO_2^{2+} adsorption onto HCSs and HCSs-oxime ($C_0 = 50$ mg L^{-1}, pH 6.0, $V = 100$ mL, $T = 298.15$ K, and $m = 10$ mg)

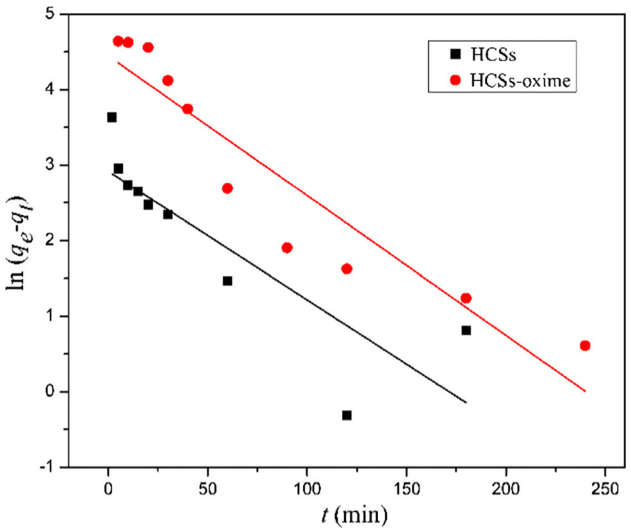

Fig. 8 Pseudo-first-order adsorption kinetic of UO_2^{2+} over HCSs and HCSs-oxime

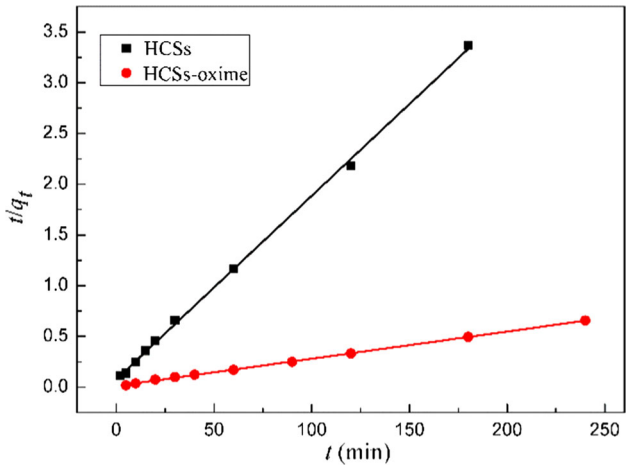

Fig. 9 Pseudo-second-order adsorption kinetic of UO_2^{2+} over HCSs and HCSs-oxime

duo to the higher active site availability for UO_2^{2+} sorption.

In order to investigate the controlling mechanism of the adsorption process, pseudo-first-order and pseudo-second-order were applied to study process. The linear form of the two models can be expressed as followed [35]:

$$\ln(q_e - q_t) = \ln q_e - k_1 t, \tag{3}$$

$$\frac{t}{q_t} = \frac{1}{k_2 q_e^2} + \frac{t}{q_e}, \tag{4}$$

where q_e and q_t refers to the amount of UO_2^{2+} adsorbed (mg g^{-1}) at equilibrium time and any time (min), k_1 (min^{-1}) and k_2 (g mg^{-1} min^{-1}) is the rate constant of first and second order adsorption, respectively.

The k_1, k_2 and q_e are calculated from the slopes and intercepts of the lines (Figs. 8, 9), and the results are shown in Table 2. The linear correlation coefficients (R^2) of the fitting experimental data for the pseudo-second-order (>0.99) are close to 1 and higher than pseudo-first-order (<0.90). Moreover, the value of $q_{e,cal}$ (HCSs: 55.2 mg g^{-1}, HCSs-oxime: 370.4 mg g^{-1}) from pseudo-second-order was closed to the experiments (HCSs: 55.0 ± 2.1 mg g^{-1}, HCSs-oxime: 365.2 ± 12.4 mg g^{-1}). Thus, the results indicate that the pseudo-second-order model is more suitable to describe the adsorption process on HCSs and HCSs-oxime. The adsorption process is regarded as chemisorption [36].

To explore the controlling stage in sorption process, further study is carried out via intra-particle diffusion models. The model can be expressed as [37]:

$$q_t = k_{id} t^{0.5}, \tag{5}$$

where k_{id} is the intra-particle diffusion rate constant. As shown in Fig. 10, it can be seen that the adsorption of uranyl ions can be divided into two stages for HCSs and three stages for HCSs-oxime, which indicates that the processes are not controlled by intra-particle diffusion of uranyl ion into adsorbents. For HCSs, initial rapid uptake rate is due to immobilizing UO_2^{2+} ions to active sites on external surface which is controlled by surface adsorption; once it reaches saturation, the UO_2^{2+} ions began to enter into inside of particles via the pores or interstice and then are adsorbed by the interior surface. Therefore, intra-particle diffusion of UO_2^{2+} is determined to be the rate-controlling step. The adsorption equilibrium is reached as the intra-particle diffusion started to slow down. While for HCSs-oxime, in the first stage, the lower slopes of plot is attributable to the lower rate of the bulk diffusion; subsequently, a higher adsorption rate is obtained for the reason

Table 2 Kinetic parameters of UO_2^{2+} adsorption onto HCSs and HCSs-oxime

Adsorbents	$q_{e,exp}$ (mg g^{-1})	Pseudo-first-order kinetics			Pseudo-second-order kinetics			Intra-particle diffusion	
		$q_{e,cal}$ (mg g^{-1})	k_1 (min^{-1})	R^2	$q_{e,cal}$ (mg g^{-1})	k_2 (g mg^{-1} min^{-1})	R^2	K_{id}	R^2
HCSs	55.0	18.4	1.7×10^{-2}	0.70	55.2	4.2×10^{-3}	0.99	3.03	0.67
HCSs-oxime	365.2	85.3	1.9×10^{-2}	0.87	370.4	5.8×10^{-4}	0.99	13.52	0.90

that the UO_2^{2+} ions start to enter into the channels of HCSs-oxime; finally, when the adsorbent is saturated, the adsorption goes to slow down.

Sorption isotherm

To study adsorption isotherms of HCSs and HCSs-oxime, different initial UO_2^{2+} concentrations solution in the range varying from 0 to 180 mg L^{-1} are utilized. The results in Fig. 11 show that the amounts of UO_2^{2+} adsorbed increase with the rising of initial UO_2^{2+} concentrations until 70 mg L^{-1} for HCSs and 160 mg L^{-1} for HCSs-oxime. This may be attributing to with the increasing initial concentration of uranyl ions in the solution, the driving force of concentration gradient overcome the diffusion resistance between the solution and solid phase.

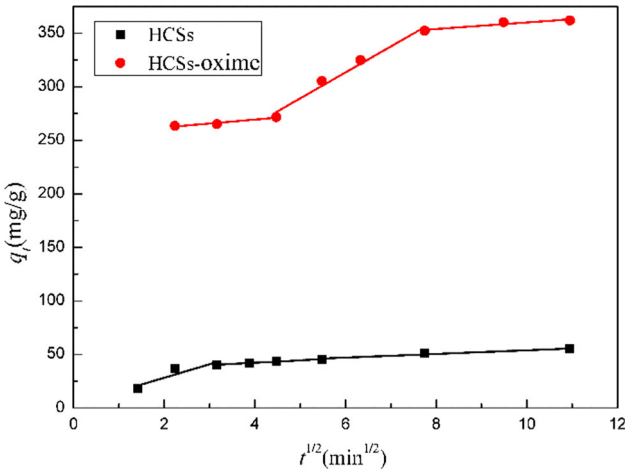

Fig. 10 Intra-particle diffusion model fitting plots for the UO_2^{2+} uptake by HCSs and HCSs-oxime

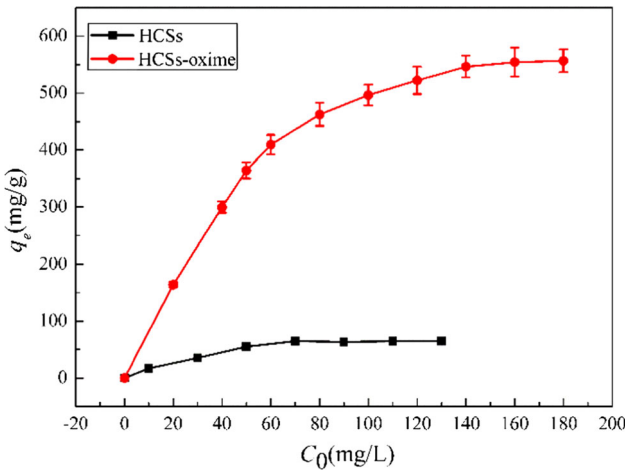

Fig. 11 Adsorption isotherm of UO_2^{2+} on HCSs and HCSs-oxime (pH 6.0, $t = 60$ min, $V = 100$ mL, $T = 298.15$ K, and $m = 10$ mg)

The sorption data were fitted using the three types of frequently used isotherms, namely Langmuir, Freundlich and Dubinin–Radushkevich (D–R) models. The Langmuir isothermal model assumes the adsorption was monolayer adsorption [38], the adsorption capacity on the surface of sorbents is the same. It can be expressed as followed:

$$\frac{C_e}{q_e} = \frac{1}{q_m K_L} + \frac{C_e}{q_m}, \tag{6}$$

where K_L is the constant relating to the energy of sorption and q_m is the maximum sorption capacity (mg g^{-1}).

The Freundlich model regards the adsorption as a multilayer sorption on a heterogeneous surface [39]. It can be expressed as followed:

$$\ln q_e = \ln K_F + \frac{1}{n} \ln C_e \tag{7}$$

where K_F is the constant relating to the capacity of sorption and n is the constant relating to the intensity of sorption.

The D–R equation is mostly employed to state the adsorption mechanism with a Gaussian energy distribution onto a heterogeneous surface [40]. The D–R isotherm can be expressed as followed:

$$\ln x = \ln x_m - K_{D-R}\varepsilon^2, \tag{8}$$

where x is the amount of uranium sorbed per mass of sorbents (mol g^{-1}), x_m is the theoretical sorption capacity (mol g^{-1}), K_{D-R} (mol^2 kJ^{-2}) is the constant related to the sorption energy and ε is the Polanyi potential, which could be calculated as followed:

$$\varepsilon = RT \ln\left(1 + \frac{1}{C_e}\right), \tag{9}$$

where R is the gas constant (8.314×10^{-3} kJ mol^{-1} K^{-1}).

The mean sorption energy (E_{D-R}, kJ mol^{-1}) could be obtained from the following Eq. (10):

$$E_{D-R} = \frac{1}{\sqrt{-2K_{D-R}}}. \quad (10)$$

The parameters calculated from the linear curves (Figs. 12, 13, 14) are listed in Table 3. For the two kinds of sorbents, it can be seen the Langmuir model fit best to the experimental data with correlation coefficients of 0.98 and 0.99, suggesting that the adsorption process is mainly dominated by monolayer sorption. The monolayer saturated adsorption capacity of HCSs-oxime is calculated to be 588.2 mg g^{-1} which is much greater than HCSs' (80.0 mg g^{-1}). Furthermore, the adsorption ability of some kinds of hydrothermal carbon modified with different functional groups published in the literatures is compared with HCSs-oxime in the Table 4 including the adsorption capacity and optimal experimental conditions. The adsorption capacity of HCSs-oxime is 588.2 mg g^{-1} which is some larger than the maximum one (466.0 mg g^{-1}, amidoxime-grafted HTC). The results indicate that the oxime group grafted on the surface play a significantly role in improving the adsorption capacity of HCSs. Meanwhile, the value of K_L of HCSs-oxime (0.11) is higher than the HCSs' (0.05), which also suggests that HCSs-oxime shows a stronger affinity toward uranyl ion. In addition, E_{D-R} value of UO_2^{2+} sorption on HCSs and HCSs-oxime were calculated to be 10.66and 13.36 kJ mol^{-1}, respectively. The result show that the sorption of uranium onto HCSs and HCSs-oxime is mainly controlled by chemical sorption [41].

Sorption thermodynamics

The effect of temperature on the adsorption of uranium onto HCSs and HCSs-oxime were studied at 288.15, 298.15 and 308.15 K. Three basic thermodynamic parameters, free energy change (ΔG), enthalpy change (ΔH) and entropy change (ΔS), were calculated using the following Eq. (11) from the experimental data and the results are shown in Table 3. Meanwhile, according to Eq. (12), a plot of ln K_d versus $1/T$ (Fig. 15) showed that K_d increased with increasing temperature in the range of 283.15–333.15 K.

$$\Delta G = \Delta H - T\Delta S, \quad (11)$$

$$\ln K_d = \frac{\Delta S}{R} - \frac{\Delta H}{RT}, \quad (12)$$

where R is the gas constant (8.314 J K^{-1} mol^{-1}).

It can be seen in Table 5, the positive value of ΔH and ΔS indicated that the adsorption of UO_2^{2+} onto HCSs and HCSs-oxime are endothermic and randomness increase process at solid–solution interface. The negative values of

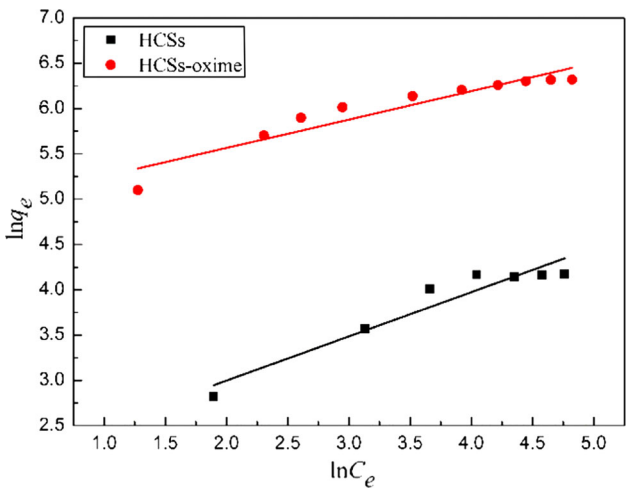

Fig. 13 Freundlich isotherms of UO_2^{2+} adsorbed on HCSs and HCSs-oxime

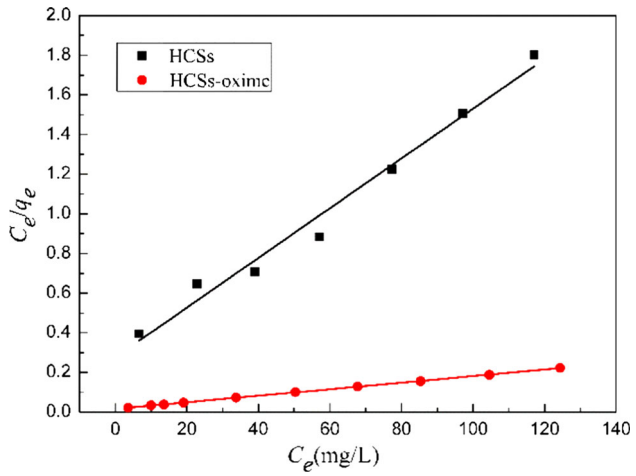

Fig. 12 Langmuir isotherms of UO_2^{2+} adsorbed on HCSs and HCSs-oxime

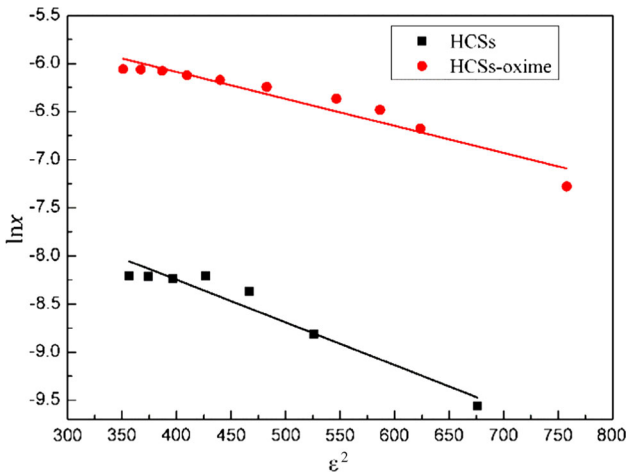

Fig. 14 D–R isotherms of UO_2^{2+} adsorbed on HCSs and HCSs-oxime

Table 3 Parameters of Langmuir, Freundlich and D–R isotherm for adsorption of UO_2^{2+} onto HCSs and HCSs-oxime

Adsorbents	Langmuir adsorptionisotherm			Freundlich adsorptionisotherm			D–R adsorption isotherm			
	K_L	q_m	R^2	K_F	n	R^2	x_m	K_{D-R}	E_{D-R}	R^2
HCSs	0.05	80.0	0.98	7.55	2.05	0.92	1.54×10^{-3}	−0.0044	10.66	0.93
HCSs-oxime	0.11	588.2	0.99	139.55	3.19	0.89	7.00×10^{-3}	−0.0028	13.36	0.92

Table 4 The comparison of adsorption capacity for HCSs-oxime with other adsorbents

Sorbents	Experimental conditions	Capacity (mg g^{-1})	Ref.
Carboxyl-rich HCSs	pH 7.0, $T = 298.15$ K	180.0	[18]
HCSs-PO_4	pH 5.0 $T = 298.15$ K	285.7	[17]
HTC-btg	pH 4.5, $T = 298.15$ K	307.3	[35]
5-azacytosine-functionalized HTC (HTC-Acy)	pH 4.5, $T = 333.15$ K	408.4	[24]
Amidoxime-grafted HTC (AO-HTC-DAMN)	pH 4.5, $T = 293.15$ K	466.0	[20]
HCSs-oxime	pH 6.0, $T = 298.15$ K	588.2	This work

ΔG demonstrate spontaneous processes for removal of UO_2^{2+} in the water. Furthermore, the larger absolute value of ΔG at higher temperature suggested that the UO_2^{2+} sorption are favor of greater temperatures [20]. Under the same experiment condition, the lower value of ΔG adsorption of UO_2^{2+} on HCSs-oxime suggested that it has a stronger sorption performance of UO_2^{2+} [19].

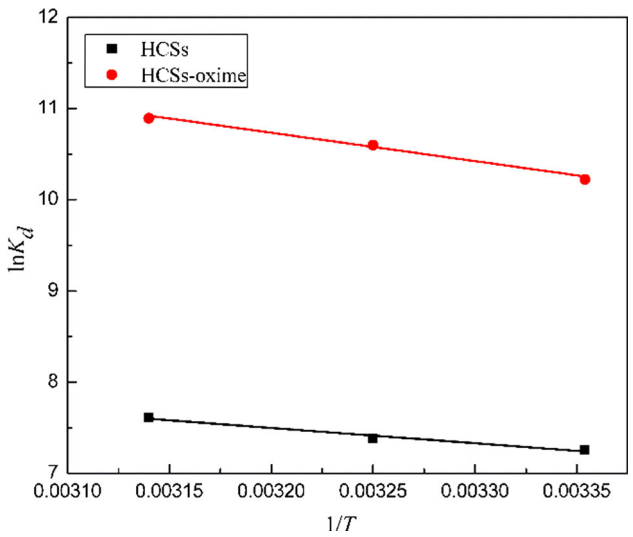

Fig. 15 The variation of ln K_d versus $1/T$ for adsorption of UO_2^{2+} on HCSs and HCSs-oxime ($C_0 = 50$ mg L^{-1}, pH 6.0, $t = 60$ min, $V = 100$ mL, and $m = 10$ mg)

Selective adsorption

The sorption selectivity of HCSs and HCSs-oxime for UO_2^{2+} was performed in a simulated nuclear industrial effluent with nine kinds of co-existing ions. The experimental conditions are the initial pH value of 6.0, contact time of 120 min, aqueous solution volume of 150 mL and temperature of 298.15 K with the initial concentration of ions 10 mg L^{-1} and the sorbents dosage of 40 mg. Results were shown in Fig. 16a, b, the adsorption capacity of UO_2^{2+} onto HCSs-oxime is 0.153 ± 0.006 mmol g^{-1} which is 2.5 times superior to HCSs (0.064 ± 0.001 mmol g^{-1}). The amounts of Mg^{2+}, Na^+, Zn^{2+}, Mn^{2+}, Co^{2+}, Ni^{2+} and Sr^{2+} adsorbed on HCSs also increase after graftation of 4-aminoacetophenone oxime group as seen from Fig. 16a. However, the distribution coefficients of HCSs-oxime (1.40×10^5) calculated for uranyl ions is two orders of magnitude better than HCSs (2.55×10^3), which suggests that HCSs functionalized with 4-aminoacetophenone oxime group show a stronger affinity toward UO_2^{2+}

Table 5 The thermodynamic parameters for adsorption of UO_2^{2+} onto HCSs and HCSs-oxime

Adsorbents	ΔH (kJ mol^{-1})	ΔS (J K^{-1} mol^{-1})	ΔG (kJ mol^{-1})		
			288.15 K	298.15 K	308.15 K
HCSs	12.44	101.89	−16.90	−17.92	−18.94
HCSs-oxime	26.47	174.00	−25.40	−27.14	−28.88

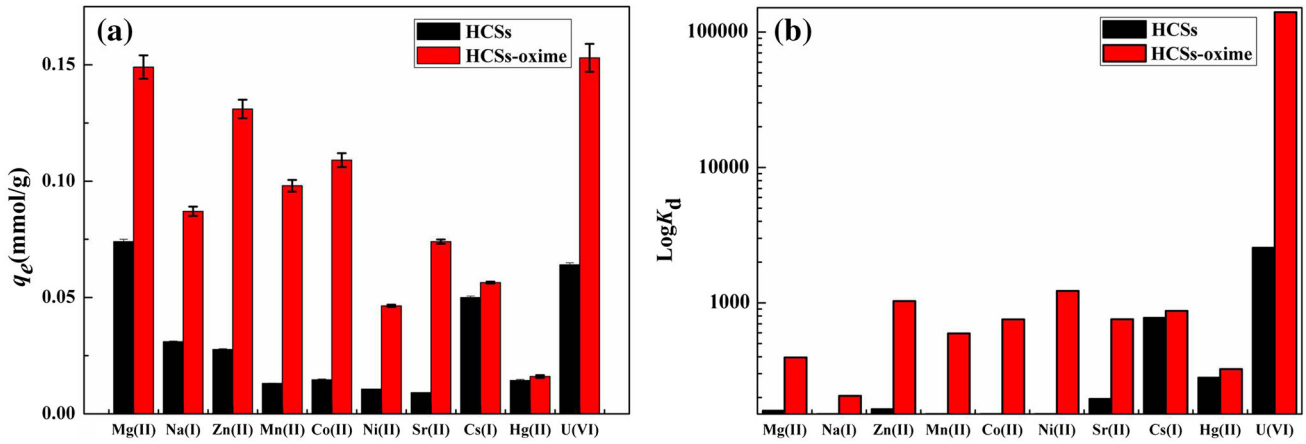

Fig. 16 **a** Competitive sorption capacities of HCSs and HCSs-oxime for UO_2^{2+} over competing ions in a simulated nuclear industrial effluent and **b** The log K_d of coexisting ions of U(VI) on HCSs and HCSs-oxime (C_0 = 10 mg L^{-1}, pH 6.0, t = 60 min, V = 150 mL, T = 298.15 K, and m = 40 mg)

The selectivity coefficient ($S_{UO_2^{2+}/M^{n+}}$) and relative selectivity coefficient (S_r) were introduced to further investigate the sorption selectivity of HCSs and HCSs-oxime for UO_2^{2+}. The two kinds of coefficients were calculated using the following Eqs. (13) and (14) from the experimental data and listed in Table 6.

$$S_{UO_2^{2+}/M^{n+}} = \frac{K_d^{UO_2^{2+}}}{K_d^{M^{n+}}}, \quad (13)$$

$$S_r = \frac{S_{HCSs-oxime}}{S_{HCSs}}, \quad (14)$$

where $K_d^{UO_2^{2+}}$ and $K_d^{M^{n+}}$ are distribution coefficients of uranyl ion and other ions, respectively.

From the results shown in Table 6, the value of relative selectivity coefficient of HCSs-oxime for Mg^{2+}, Cs^+ and Hg^{2+} are more than 22.00, and other ions are more than 4.00. The results above indicate that the adsorptive selectivity of uranium is significantly improved after graftion of oxime group on HCSs.

Table 6 Distribution coefficient and selectivity coefficients of HCSs and HCSs-oxime

Elements	K_d (mL g^{-1})		S		S_r
	HCSs	HCSs-oxime	HCSs	HCSs-oxime	
U(VI)	2552.63	140,052.48	–	–	–
Mg(II)	159.84	394.95	15.97	354.61	22.20
Na(I)	64.87	205.76	39.35	680.66	17.30
Zn(II)	164.24	1031.07	15.54	135.83	8.74
Mn(II)	78.81	595.31	32.39	235.26	7.26
Co(II)	85.78	755.07	29.76	185.48	6.23
Ni(II)	92.89	1226.48	27.48	114.19	4.16
Sr(II)	195.33	756.42	13.07	185.15	14.17
Cs(I)	775.35	872.86	3.29	160.45	48.74
Hg(II)	280.04	324.63	9.12	431.42	47.33

Desorption and reusability study

Desorption and reusability study of HCSs-oxime has been appended to this work, results are shown in Fig. 17. In this work, desorption experiments of U(VI) were studied in different concentration of HCl solution (0.01–0.09 mol L^{-1}). As shown in Fig. 17a, with the increasing of concentration of eluent HCl solution from 0.01 to 0.09 mol L^{-1} HCl, the desorption efficiency increase from 57.2 ± 1.0 to 96.5 ± 3.1%, hence the 0.09 mol L^{-1} HCl solution was chosen as optimal condition for recovery of uranium from the adsorbed HCSs-oxime. The adsorbents after desorption was regenerated by washing to nearly neutral with the distilling water. The adsorption–desorption cycle was repeated five times to investigate the reusability properties and the results were presented in Fig. 17b. The adsorption capacity of U(VI) was decreased slightly form 368.8 ± 14.5 to 339.3±9.2 mg g^{-1}, suggested that HCSs-oxime can be used for over five times of adsorption–desorption recycle.

Possible sorption mechanism

According to various references [33, 42], the adsorbents with oxime group show excellent adsorption capacity and selectivity toward uranium. The sorption mechanism of UO_2^{2+} on HCSs-oxime is present in Scheme 2. The fixation of UO_2^{2+} is relevant to both nitrogen and oxygen in 4-aminoacetophenone oxime group.

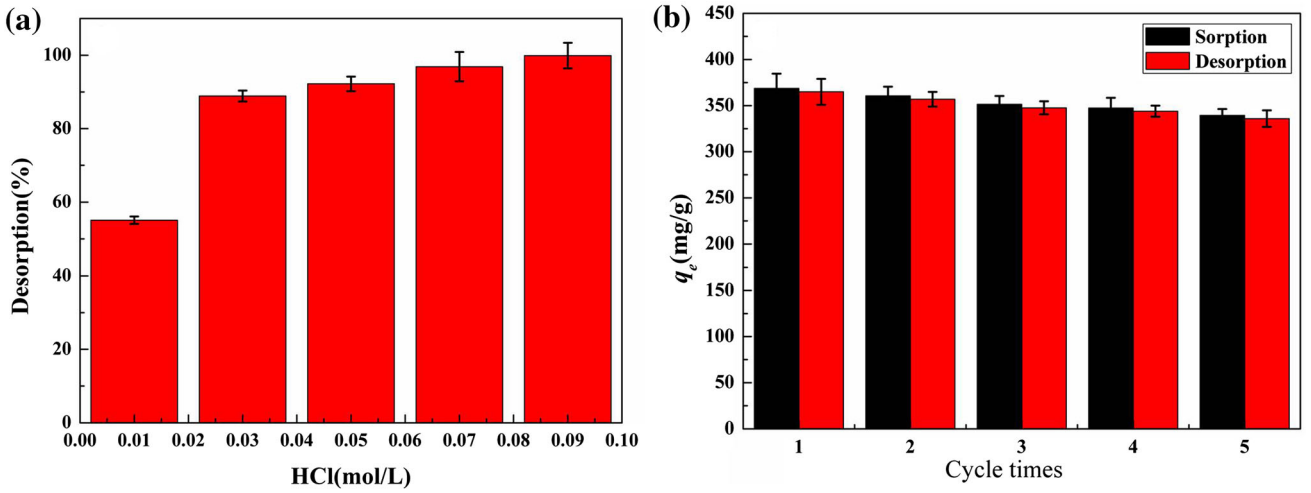

Fig. 17 **a** Effect of HCl concentration on desorption of UO_2^{2+} sorbed by HCSs-oxime and **b** reusability of HCSs-oxime for removal of UO_2^{2+}

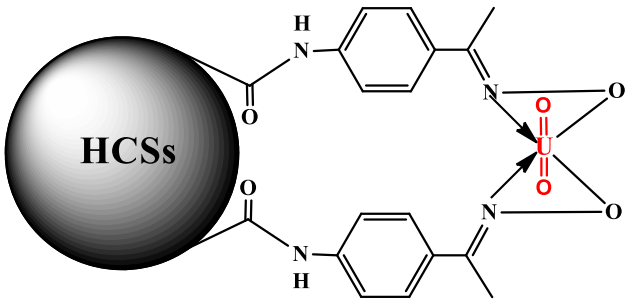

Scheme 2 Probable sorption mechanism of UO_2^{2+} on HCSs-oxime

Conclusions

HCSs-oxime has been successfully prepared by covalently anchoring 4-aminoacetophenone oxime onto HCSs. The optimal initial solution pH and contact time is determined to be 6.0 and 60 min for HCSs-oxime to adsorb of UO_2^{2+}, respectively. Simultaneously, sorption of uranyl ion on HCSs-oxime can be explained by Langmuir and pseudo-second model indicating a chemical controlled adsorption processes. The maximum monolayer adsorption capacity increasing from 80.0 to 588.2 mg g^{-1} after 4-aminoacetophenone oxime-grafting. In addition, the adsorptive selectivity for uranium is significantly improved after modified with 4-aminoacetophenone oxime. The results indicate that the HCSs-oxime is a potentially effective adsorbent for removal UO_2^{2+} in aqueous solution.

Acknowledgements This work was financially supported by the National Natural Science Foundation of China (Grant Nos. 21561002, 21301028, 11475044, 41461070, 21401022), the Program for Changjiang Scholars and Innovative Research Team in University (Grant No. IRT13054), the Science and Technology Support Program of Jiangxi Province (Grant Nos. 20141BBG70001, 20151BBG70010), the Advanced Science and Technology Innovation Team Program of Jiangxi Province (Grant No. 20142BCB24006), the Innovation Fund of Graduate Student (DHYC-2016010), and the Innovation Team Program of Jiangxi Provincial Department of Science and Technology (Grant No. 2014BCB24006).

References

1. Liu J, Zhao C, Zhang Z et al (2016) Fluorine effects on U(VI) sorption by hydroxyapatite. Chem Eng J 288:505–515
2. Reinoso-Maset E, Ly J (2016) Study of uranium(VI) and radium(II) sorption at trace level on kaolinite using a multisite ion exchange model. J Environ Radioact 157:136–148
3. Shao L, Wang X, Ren Y et al (2016) Facile fabrication of magnetic cucurbit[6]uril/graphene oxide composite and application for uranium removal. Chem Eng J 286:311–319
4. Zhou L, Wang Y, Zou H et al (2016) Biosorption characteristics of uranium(VI) and thorium(IV) ions from aqueous solution using $CaCl_2$-modified Giant Kelp biomass. J Radioanal Nucl Chem 307(1):635–644
5. Hoyer M, Zabelt D, Steudtner R et al (2014) Influence of speciation during membrane treatment of uranium contaminated water. Sep Purif Technol 132:413–421
6. Tan L, Zhang X, Liu Q et al (2015) Preparation of magnetic core–shell iron oxide@silica@nickel–ethylene glycol microspheres for highly efficient sorption of uranium(VI). Dalton Trans 44:6909–6917
7. Mishra S, Dwivedi J, Kumar A et al (2015) Studies on salophen anchored micro/meso porous activated carbon fibres for the removal and recovery of uranium. RSC Adv 5:33023–33036
8. Wang YL, Song LJ, Zhu L et al (2014) Removal of uranium(VI) from aqueous solution using iminodiacetic acid derivative functionalized SBA-15 as adsorbents. Dalton Trans 43:3739–3749
9. Zhang ZB, Yu XF, Cao XH et al (2014) Adsorption of U(VI) from aqueous solution by sulfonated ordered mesoporous carbon. J Radioanal Nucl Chem 301:821–830
10. Chen S, Hong J, Yang H et al (2013) Adsorption of uranium(VI) from aqueous solution using a novel graphene oxide-activated carbon felt composite. J Environ Radioact 126:253–258
11. Yan H, Bai J, Chen X et al (2013) High U(VI) adsorption capacity by mesoporous $Mg(OH)_2$ deriving from MgO hydrolysis. RSC Adv 3:23278
12. Cao Q, Liu Y, Wang C et al (2013) Phosphorus-modified poly(styrene-co-divinylbenzene)-PAMAM chelating resin for the

adsorption of uranium(VI) in aqueous. J Hazard Mater 263(Pt 2):311–321
13. Wang Z, Zachara JM, Shang J et al (2014) Investigation of U(VI) adsorption in quartz–chlorite mineral mixtures. Environ Sci Technol 48:7766–7773
14. Olivelli MS, Curutchet GA, Torres Sánchez RM (2013) Uranium uptake by montmorillonite–biomass complexes. Ind Eng Chem Res 52:2273–2279
15. Zhang ZB, Zhou ZW, Cao XH et al (2013) Removal of uranium(VI) from aqueous solutions by new phosphorus-containing carbon spheres synthesized via one-step hydrothermal carbonization of glucose in the presence of phosphoric acid. J Radioanal Nucl Chem 299:1479–1487
16. Mi Y, Hu W, Dan Y et al (2008) Synthesis of carbon microspheres by a glucose hydrothermal method. Mater Lett 62:1194–1196
17. Yao C, Shin Y, Wang LQ et al (2007) Hydrothermal dehydration of aqueous fructose solutions in a closed system. J Phys Chem C 111:15141–15145
18. Zhang ZB, Nie WB, Li Q et al (2013) Removal of uranium(VI) from aqueous solutions by carboxyl-rich hydrothermal carbon spheres through low-temperature heat treatment in air. J Radioanal Nucl Chem 298:361–368
19. Yu XF, Liu YH, Zhou ZW et al (2014) Adsorptive removal of U(VI) from aqueous solution by hydrothermal carbon spheres with phosphate group. J Radioanal Nucl Chem 300:1235–1244
20. Geng J, Ma L, Wang H et al (2012) Amidoxime-grafted hydrothermal carbon microspheres for highly selective separation of uranium. J Nanosci Nanotechnol 12:7354–7363
21. Zhao Y, Wang X, Li J et al (2015) Amidoxime functionalization of mesoporous silica and its high removal of U(VI). Polym Chem 6:5376–5384
22. Zhang Z, Dong Z, Dai Y et al (2016) Amidoxime-functionalized hydrothermal carbon materials for uranium removal from aqueous solution. RSC Adv 6:102462–102471
23. Zou YD, Cao XH, Luo XP et al (2015) Recycle of U(VI) from aqueous solution by situ phosphorylation mesoporous carbon. J Radioanal Nucl Chem 306:515–525
24. Song Q, Ma L, Liu J et al (2012) Preparation and adsorption performance of 5-azacytosine-functionalized hydrothermal carbon for selective solid-phase extraction of uranium. J Colloid Interface Sci 386:291–299
25. Aakeröy CB, Beatty AM, Leinen DS (2001) Syntheses and crystal structures of new extended building blocks for crystal engineering: (pyridylmethylene)aminoacetophenone oxime ligands. Cryst Growth Des 1:47–52
26. Nie BW, Zhang ZB, Cao XH et al (2013) Sorption study of uranium from aqueous solution on ordered mesoporous carbon CMK-3. J Radioanal Nucl Chem 295:663–670
27. Tripathi A, Melo JS, D'Souza SF (2013) Uranium(VI) recovery from aqueous medium using novel floating macroporous alginate–agarose–magnetite cryobeads. J Hazard Mater 246:87–95
28. Zare F, Ghaedi M, Daneshfar A et al (2015) Efficient removal of radioactive uranium from solvent phase using AgOH–MWCNTs nanoparticles: kinetic and thermodynamic study. Chem Eng J 273:296–306
29. Chen Z, Ma L, Li S et al (2011) Simple approach to carboxyl-rich materials through low-temperature heat treatment of hydrothermal carbon in air. Appl Surf Sci 257:8686–8691
30. Shen H, Pan S, Zhang Y et al (2012) A new insight on the adsorption mechanism of amino-functionalized nano-Fe_3O_4 magnetic polymers in Cu(II), Cr(VI) co-existing water system. Chem Eng J 183:180–191
31. He L, Dumée LF, Feng C et al (2015) Promoted water transport across graphene oxide–poly(amide) thin film composite membranes and their antibacterial activity. Desalination 365:126–135
32. Wang Y, Gu Z, Yang J et al (2014) Amidoxime-grafted multiwalled carbon nanotubes by plasma techniques for efficient removal of uranium(VI). Appl Surf Sci 320:10–20
33. Tian G, Geng J, Jin Y et al (2011) Sorption of uranium(VI) using oxime-grafted ordered mesoporous carbon CMK-5. J Hazard Mater 190:442–450
34. Zhao Y, Li J, Zhang S et al (2014) Amidoxime-functionalized magnetic mesoporous silica for selective sorption of U(VI). RSC Adv 4:32710–32717
35. Li B, Ma L, Tian Y et al (2014) A catechol-like phenolic ligand-functionalized hydrothermal carbon: one-pot synthesis, characterization and sorption behavior toward uranium. J Hazard Mater 271:41–49
36. Yuan D, Chen L, Xiong X et al (2016) Removal of uranium(VI) from aqueous solution by amidoxime functionalized superparamagnetic polymer microspheres prepared by a controlled radical polymerization in the presence of DPE. Chem Eng J 285:358–367
37. Zhang S, Zhao X, Li B et al (2016) "Stereoscopic" 2D supermicroporous phosphazene-based covalent organic framework: design, synthesis and selective sorption towards uranium at high acidic condition. J Hazard Mater 314:95–104
38. Boparai HK, Joseph M, O'Carroll DM (2011) Kinetics and thermodynamics of cadmium ion removal by adsorption onto nano zero valent iron particles. J Hazard Mater 186:458–465
39. Pillewan P, Mukherjee S, Roychowdhury T et al (2011) Removal of As(III) and As(V) from water by copper oxide incorporated mesoporous alumina. J Hazard Mater 186:367–375
40. Budnyak TM, Strizhak AV, Gładysz-Płaska A et al (2016) Silica with immobilized phosphinic acid-derivative for uranium extraction. J Hazard Mater 314:326–340
41. Zhang X, Jiao C, Wang J et al (2012) Removal of uranium(VI) from aqueous solutions by magnetic Schiff base: kinetic and thermodynamic investigation. Chem Eng J 198:412–419
42. Gunathilake C, Górka J, Dai S et al (2015) Amidoxime-modified mesoporous silica for uranium adsorption under seawater conditions. J Mater Chem A 3:11650–11659